Low-Field Magnetoresistance in $La_{0.67}Sr_{0.33}MnO_3$:ZnO Composite Film

*Margo Staruch, Haiyong Gao, Pu-Xian Gao, and Menka Jain**

A nanocomposite film of $La_{0.67}Sr_{0.33}MnO_3$ (LSMO):ZnO is synthesized by depositing LSMO solution on a vertical array of ZnO nanorods grown on (0001) Al_2O_3 substrate. The magnetic behavior of the composite film differs from that of a pure LSMO film, possibly due to smaller grain size in the composite, small amount of Zn doping, or the presence of nonmagnetic ZnO phase near the LSMO grain boundaries. Magnetotransport measurements show that the low-field magnetoresistance (LFMR) of the nanocomposite film is significantly enhanced as compared to that observed for pure LSMO film. The highest value of the LFMR of the nanocomposite film at 10 K is –23.9% with a magnetic field of 0.5 T applied parallel to the current.

1. Introduction

Hole-doped pervoskite manganites such as $La_{1-x}Sr_xMnO_3$ (LSMO) have been of great interest due to their complex magneotransport properties. In these manganites intrinsic colossal magnetoresistance (CMR), which is a gigantic decrease of resistance by the application of an external magnetic field, is observed near the Curie temperature (T_c) with high applied magnetic fields (≥1 T).[1–3] Recently, there has been considerable research in order to achieve high magnetoresistance (MR) values with lower magnitude of the applied magnetic fields (<1 T) by taking the advantage of the extrinsic MR effect.[4–6] The extrinsic MR effect has been observed in ceramics and polycrystalline films in a wide temperature range in the ferromagnetic region (at temperatures much lower than Curie temperature). In polycrystalline LSMO and related compounds, LFMR has been obtained by structuring grain boundaries, artificial grain boundaries, nanosized inclusions, and atomic-sized defects.[7] Such low-field magnetoresistance (LFMR) has been explained by spin-polarized tunneling between adjacent grains or spin-dependent scattering at the grain boundaries.[4–6] In bulk LSMO, these studies include composites with glass,[8] CeO_2,[9] ZrO_2,[10] and ZnO[11,12] etc.. However, there have been only a few reports that present LFMR effects in such composites in thin film form.[13,14] These efforts have primarily been focused on preparing films by pulsed laser deposition (PLD) technique. For example, for a PLD grown LSMO:ZnO nanocomposite film, MR value of –12% at 77 K and 1 T was observed[13] and a LSMO:Ag composite film was reported to have a maximum MR value of –12% at 77 K and 0.4 T for a sample near the percolation threshold.[14] It should be noted that PLD method does not allow large area fabrication of such composite films and the nanocomposite structure (nanopillar or vertically aligned nanostructure) is not maintained after a certain thickness that imposes certain limitations. On the other hand, large area thick film fabrication as well as deposition on uneven surfaces is possible using solution techniques.

In the present work, we report a novel and cost-effective solution approach to fabricate a $La_{0.67}Sr_{0.33}MnO_3$:ZnO (LSMO:ZnO) composite film by combining hydrothermal method and spin-coating in an attempt to fabricate nanocomposite film with enhanced LFMR effect. For the fabrication of the composite film, La(0.67)Sr(0.33)Mn(1) solution was spin coated on to the ZnO nanorod coated substrate. The LSMO is a ferromagnetic metal (at low temperatures) and ZnO is a non-magnetic semiconductor that could favor spin-dependent tunneling in composites, which makes this combination attractive for LFMR studies.

Dr. M. Jain
Department of Physics and Institute of Materials Science
University of Connecticut,
Storrs,CT 06269, USA
E-mail: menka.jain@uconn.edu
M. Staruch
Department of Physics
University of Connecticut
Storrs, CT 06269, USA
Dr. H. Gao, Dr. P.-X. Gao
Department of Chemical Materials & Biomolecular Engineering and Institute of Materials Science
University of Connecticut
Storrs, CT 06269, USA

DOI: 10.1002/adfm.201200489

2. Results and Discussion

The X-ray diffraction (XRD) θ–2θ pattern of the composite film (as shown in **Figure 1**) shows the presence of (110), (111), (024), and (211) diffraction peaks of the LSMO phase. Stronger (110) peak as compared to several other weaker peaks of different orientations indicate that the LSMO phase is preferentially oriented along (110) direction. The pseudocubic lattice parameters of LSMO phase in pure LSMO and composite films are 3.857 Å and 3.871 Å, respectively. These values are smaller but close to the bulk lattice parameter for LSMO (3.873 Å), indicating that the composite film is relaxed.[15] Ju et al. reported an increase in lattice parameter values of similar manganites with increasing oxygen vacancies.[16] However, lower lattice parameters in the

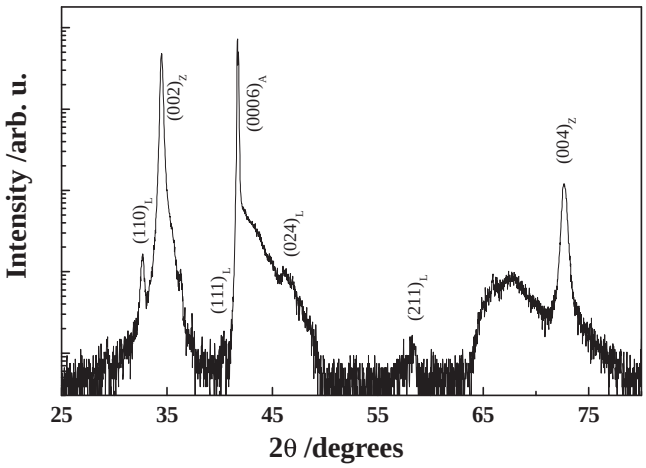

Figure 1. θ–2θ scan of LSMO:ZnO composite film. Here L, Z, and A represent peaks of LSMO, ZnO, and Al_2O_3 respectively.

present films may indicate the absence of oxygen vacancies in the films. A strong (0001) peak of ZnO indicates that the ZnO nanorods are highly *c*-axis oriented. The out-of-plane lattice parameter of ZnO was calculated to be $c = 5.194$ Å, which is close to the previously reported value of $c = 5.207$ Å.[17] The average crystallite size (D) of the LSMO phase was calculated using Scherrer's equation, $D = 0.9\lambda/\beta\cos\theta$, where λ is the wavelength of the X-ray source, β is the full width at half maximum, and θ is the Bragg angle. The values of D are 29.25 nm for the present LSMO film and 20.54 nm for LSMO:ZnO composite film. This result shows that the average crystallite size of the LSMO phase reduces in the present composite film.

The cross-sectional scanning electron microscopy (SEM) images of the as-grown ZnO nanorods and the LSMO:ZnO composite film are shown in **Figure 2**a and (b), respectively. From the cross-sectional images it is clear that using the present solution technique, LSMO phase fills up the volume between the ZnO nanorods and no pores are observed. The thickness of the composite film is ~400 nm that is defined by the length of

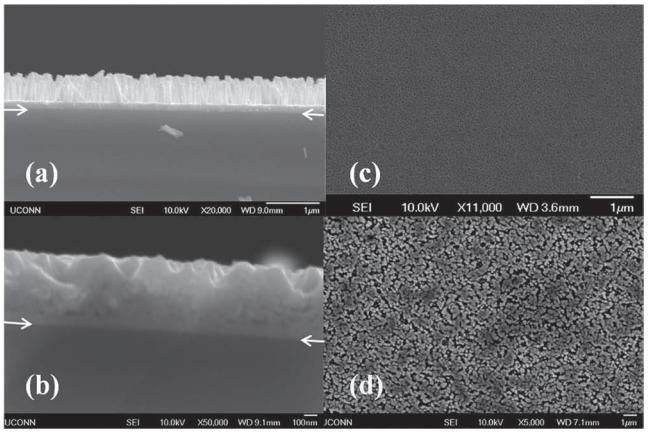

Figure 2. Cross-sectional SEM images of (a) ZnO nanorods and (b) LSMO:ZnO composite film on substrate, and top-view SEM images of (c) LSMO film and (d) LSMO:ZnO composite film. Arrows indicate the interface between ZnO seed layer and substrate.

the starting ZnO nanorods. Comparing the top view of the pure and composite film in Figure 2c and d respectively, it is inferred that the grain size of LSMO is smaller in the composite film as compared to that in the pure film. The ZnO nanorods were found to have a diameter of 60–80 nm and an average spacing of 30–50 nm. This spacing between the nanorods should be a limiting factor for grain size. Thus LSMO phase fills roughly 1/3 of the total volume of the composite film. It has also been observed in LSMO:ZnO ceramic composites that a small amount of Zn may substitute for Mn at LSMO/ZnO interface.[18] Therefore, a small compositional variation at the interfaces may also modify the grain boundaries in the present composite film.[12]

The zero field cooled (ZFC) and field cooled (FC) magnetization values (at 100 Oe field) normalized to magnetization at 10 K $\{M(T)/M(10\text{ K})\}$ are plotted as a function of temperature in **Figure 3**a. The magnetization value at 10 K for the composite film is 1.7×10^{-4} emu cm^{-3}. This value is smaller than that for the pure LSMO film (2.3×10^{-4} emu cm^{-3}), which may be due to grain-size effects.[7,10,19] It is generally assumed that the ferromagnetic coupling among the Mn-ions in the grain boundary region is much weaker than among Mn-ions in the grain core.[5,20–22] In the present composite film, due to smaller grain size, the volume fraction of grain boundaries in the overall film is larger than that of the pure film. Thus, overall ferromagnetic coupling could be weaker in the present composite film.

The temperature coefficient of the FC magnetization data, defined as TCM = $1/M(dM/dT)$, is plotted in Figure 3b as a function of temperature. A peak in TCM vs. temperature plot is generally observed at the ferromagnetic transition temperature (T_c).[10,23] A sharp peak at 360 K and a broader peak at 315 K are observed in the TCM plots for the pure LSMO and composite films, respectively. It is believed that slight magnetic or compositional disorder in the grain boundary region as compared to the core of the grain that could result in a broader peak in the present composite film.[24] In that case, below the transition temperature, the grain boundary composition could still be in the paramagnetic phase as compared to the ferromagnetic phase in the core of the grain giving rise to a broad transition temperature. In addition, the presence of nonmagnetic and semiconductor ZnO near the LSMO grains can further induce the magnetic disorder at the grain boundaries and dilute the double exchange,[21,25] which could explain the broadening and lowering of the TCM peak. Similar broadening and decrease in transition temperature has been reported for manganite:insulator composites.[10] Magnetization vs. magnetic field data (not shown) of the composite film shows ferromagnetic behavior with a coercive field (H_c) of 240 Oe at 10 K. It should be noted that Balcells et al. observed an increase in H_c at 10 K in LSMO ceramic sample with reducing particle size.[26] The higher value of coercive field in the present composite film as compared to values observed for polycrystalline films in the literature (~200 Oe) could indicate that the small-size LSMO grains behave essentially as magnetic single domains.[24]

In epitaxial films and single crystals of LSMO, metal-insulator transition ($T_{M\text{-}I}$) and T_c occur at nearly the same temperature.[1,7–8] Temperature dependent resistivity (ρ) values of the present pure LSMO and composite films are shown in Figure 3b. A well-defined $T_{M\text{-}I}$ {defined as the temperature at the peak in $\rho(T)$ data} was observed for both films. Three

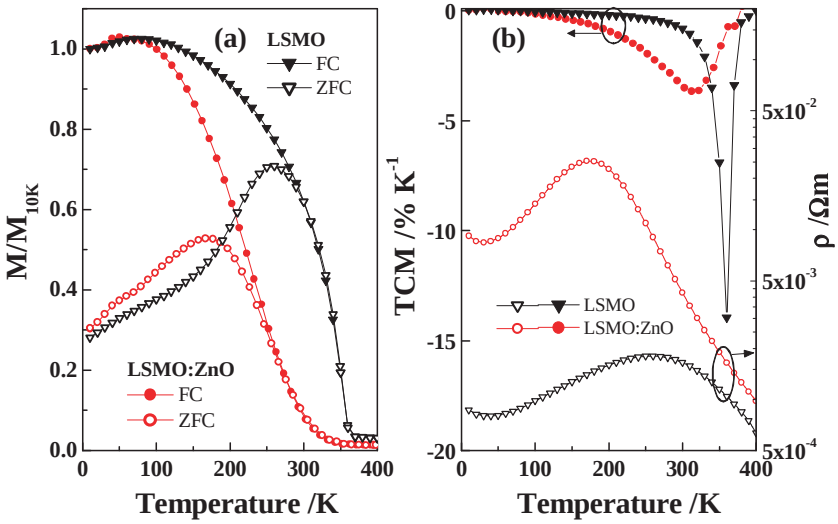

Figure 3. (a) ZFC and FC magnetization as a function of temperature normalized to value at 10 K for LSMO film and LSMO:ZnO composite film, and (b) TCM and resistivity values for LSMO and LSMO:ZnO films.

important observations in these plots are: (i) the $T_{M\text{-}I}$ of the composite film (~170 K) shifts to lower temperature compared to the $T_{M\text{-}I}$ of the pure LSMO film (285 K), (ii) the peak resistivity of the composite film is much higher than that in the pure film, and (iii) $T_{M\text{-}I}$ of the LSMO:ZnO film is lower than the T_c of the film. It should be noted that small grains (i.e. the presence of large number of grain boundaries), interfaces between the neighboring grains, reduced domain size, inter-grain distance, increased disorder, as well as insulating phases induces barriers to the electrical transport that can explain higher resistivity and as well as the shift in $T_{M\text{-}I}$.[9,19,27,28] The increase in the resistivity and shift in $T_{M\text{-}I}$ in the present composite film may also be due to the presence of higher resistive grain-boundaries and ZnO nanorods that may affect the electronic conduction between LSMO grains. In addition, the difference in $T_{M\text{-}I}$ and T_C indicates grain-size effects.

The $\rho(T)$ values of both films were found to reduce with applied magnetic field. From the $\rho(T)$ data measured at zero and 0.5 T, magnetoresistance was calculated (MR = $100*(\rho_{0.5T}- \rho_0)/\rho_0$, where ρ_0 and $\rho_{0.5T}$ are the resistivity values at zero field and with applied field of 0.5 T, respectively). Only one maximum is observed at low temperatures in the MR vs. temperature plot (not shown here) for the LSMO:ZnO composite film at temperatures lower than T_C. Li *et al.* observed two components of MR in LSMO and $La_{0.67}Ca_{0.33}MnO_3$ films: one dominant near T_c from the regular CMR mechanism and one dominant at low temperature, due to scattering at grain boundaries.[29] In the present LSMO:ZnO composite film, absence of a peak in MR values near $T_{M\text{-}I}$ or T_c of the sample indicates that there was only one component of MR, which is from the magnetic scattering at grain boundaries. It should be noted that the MR value at 0.5 T is much higher than the present pure LSMO film.

The field dependent resistivity values $\{\rho(H)\}$ measured at low temperatures (10, 80, and 170 K) display the typical hysteresis behavior with resistivity maxima (ρ_{max}) at the respective coercive field. The out-of-plane ($H \perp I$) and in-plane ($H \parallel I$) $\rho(H)$ data was used to calculate MR $\{= (\rho_H - \rho_{max})/\rho_{max}$, where ρ_H is the resisivity values at applied field of $H\}$ and the plots at 10 K for the pure LSMO and LSMO:ZnO composite films are presented in **Figure 4**a. The out-of plane MR vs. field data shows an initial rise in MR followed by a region where MR is almost linear with field. The LSMO:ZnO composite film shows larger out-of plane MR values at all measured fields and shows a sharper drop at low fields (less than 0.5 T) as compared to the LSMO film. Such sharp drop in the MR values in composite film at low fields is believed to be due to enhanced spin-polarized tunneling between LSMO grains through modified grain boundaries and/or insulating ZnO phase. At 10 K and with applied field of 0.5 T ($H \perp I$), MR values are –8.3% and – 18.5% for the LSMO and LSMO:ZnO films, respectively. This suggests that magnetic field sensitivity can be significantly enhanced with such composite formation. Figure 4a also plots the MR value vs. applied field ($H \parallel I$) for the LSMO:ZnO composite film. It should be noted that higher values of negative MR with smaller magnetic fields were obtained when the field was parallel to current. This anisotropic behavior of the

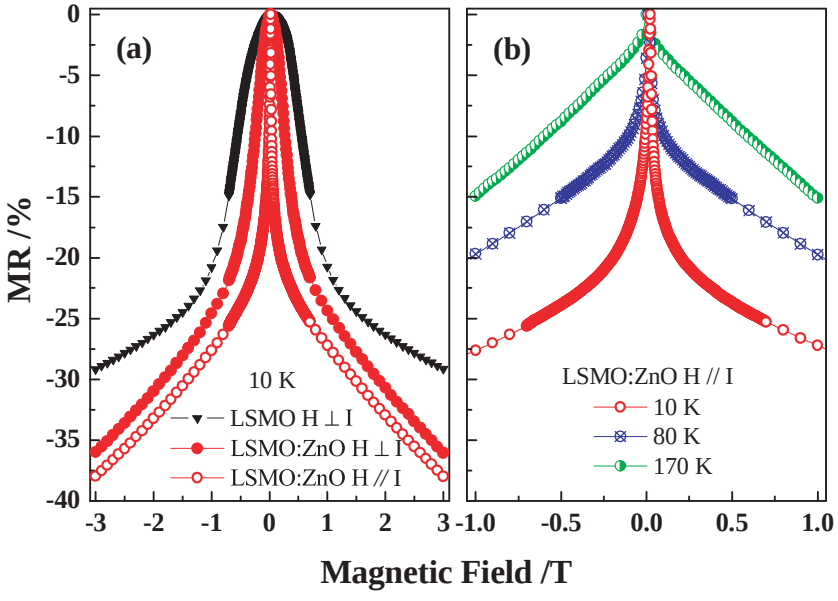

Figure 4. Magnetoresistance (MR) vs. applied magnetic field (a) at 10 K with field perpendicular to current for LSMO and LSMO:ZnO films, and parallel to current for LSMO:ZnO composite film, and (b) parallel to current for LSMO:ZnO composite film at 10 K, 80 K, and 170 K.

MR has previously been observed in polycrystalline LSMO as a result of strain and LSMO composite films as a result of reduced coupling between LSMO grains.[30,31] Sharp LFMR behavior is also found at higher temperatures (Figure 4b) with significant values of MR at low fields, and the MR values are highest at 10 K as mentioned previously. The highest value of low-field MR ($H \parallel I$) at 10 K and 0.5 T is –23.9% for the present LSMO:ZnO composite film. It should be noted that these MR values are an improvement when compared to a LSMO:Ag composite film (–14.1% vs. –12% at 0.4 T and 77 K),[14] a LSMO/STO multilayer film (–17.8% vs. –15% at 0.5 T and 20 K),[32] and the LSMO:ZnO film grown by PLD (–19.7% vs. –12% at 77 K and 1 T).[13] The LSMO:ZnO composite film in this work could be promising for applications, such as in magnetic field sensors due to sizeable change in MR with a small change in low magnetic fields. Thus the present composite approach opens up new pathways to grow nanocomposite films in which LFMR can further be tuned by controlling the thickness and density of the ZnO nanorods.

3. Conclusions

In summary, a novel and cost-effective approach of fabricating $La_{0.67}Sr_{0.33}MnO_3$:ZnO (LSMO:ZnO) composite thin film with high magnetic field sensitivity is presented here that combines the hydrothermal growth and spin coating techniques. The LSMO phase filled up the space between the ZnO nanorods. Modified LSMO grain boundaries and the ZnO phase at the interface of LSMO grains may be responsible to enhance spin-polarized tunneling in the composite film. This leads to a significant enhancement in low-field magnetoresistance (LFMR) in the present composite film as compared to the pure LSMO film. The field sensitivity of the MR is higher when the applied magnetic field is parallel to the direction of the current and substrate. The maximum LFMR value of –23.9% was achieved at 10 K with an applied field of as low as 0.5 T in the composite film.

4. Experimental Section

ZnO Nanorod Fabrication: An aqueous solution of zinc acetate and hexamethylenetetramine was prepared. This Zn-precursor solution was spin coated onto the (0001) oriented Al_2O_3 substrate that results in the formation of ZnO seed layer by a process involving hydrolysis and condensation. The substrate with ZnO seed layers were immersed into the solution in a container and the container was sealed and put into a water bath. After ZnO nanorod growth, the samples were taken out, rinsed, cleaned with DI water several times, and dried overnight. More details can be found in [33].

Sample Preparation: High purity precursors of La, Sr, and Mn were mixed in a stoichiometric ratio in water and ethylene glycol to prepare the La(0.67)Sr(0.33)Mn(1) solution. To prepare pure LSMO and LSMO:ZnO composite film, this solution was spin coated several times onto (0001) Al_2O_3 substrate as well as on vertically aligned ZnO nanorods coated (0001)-Al_2O_3 substrate. After each coating, the films were pyrolyzed at 600 °C for 5 minutes in oxygen. After the final coating, the films were annealed at 850 °C for 2 hours in oxygen.

Sample Characterization: X-ray diffraction measurements were performed to characterize structure of the films. Scanning electron microscopy was used to analyze the growth of ZnO nanorods and the LSMO:ZnO film. Resistivity values were measured as a function of temperature (from 10 K–400 K) and as a function of applied magnetic field {from –3 T to +3 T (–30,000 Oe to +30,000 Oe)} at 10 K and 80 K using a standard four-probe technique in a Physical Property Measurement System (Quantum Design). For out-of-plane data, resistivity was measured with magnetic field applied perpendicular to the current ($H \perp I$) as well as to the substrate and for the in-plane measurements, resistivity was measurements with magnetic field applied parallel to the current and substrate ($H \parallel I$). The magnetic moment of the films was measured as a function of temperature (from 10 K–400 K) with 100 Oe applied field with vibrating sample magnetometer.

Acknowledgements

The author M.J. is grateful to the financial support from National Science Foundation (NSF1105975).

Received: February 17, 2012
Published online: May 18, 2012

[1] A. Urushibara, Y. Moritomo, T. Arima, A. Asamitsu, G. Kido, Y. Tokura, *Phys. Rev. B* **1995**, *51*, 14103.
[2] A.-M. Haghiri-Gosnet, J.-P. Renard, *J. Phys. D. Appl. Phys.* **2003**, *36*, R127.
[3] M. Jain, E. Bauer, F. Ronning, M. F. Hundley, L. Civale, H. Wang, B. Maiorov, A. K. Burrell, T. M. McClesky, S. R. Foltyn, R. F. DePaula, Q. X. Jia, *J. Am. Ceram. Soc.* **2008**, *91*, 1858.
[4] J.-H. Park, E. Vescovo, H.-J. Kim, C. Kwon, R. Ramesh, T. Venkatesan, *Nature* **1998**, *392*, 794.
[5] N. Zhang, W. Ding, W. Zhong, D. Xing, Y. Du, *Phys. Rev. B* **1997**, *56*, 8138.
[6] P. Raychaudhuri, K. Sheshadri, P. Taneja, S. Bandyopadhyay, P. Ayyub, A. K. Nigam, R. Pinto, S. Chaudhary, S. B. Roy, *Phys. Rev. B* **1999**, *59*, 13919.
[7] H. Y. Hwang, S.-W. Cheong, N. P. Ong, B. Batlogg, *Phys. Rev. Lett.* **1996**, *77*, 2041.
[8] S. Gupta, R. Ranjit, C. Mitra, P. Raychaudhuri, R. Pinto, *Appl. Phys. Lett.* **2001**, *78*, 362.
[9] Ll. Balcells, A. E. Carrillo, B. Martínez, J. Fontcuberta, *Appl. Phys. Lett.* **1999**, *74*, 4014.
[10] B. Huang, Y. Liu, R. Zhang, X. Yuan, C. Wang, L. Mei, *J. Phys. D: Appl. Phys.* **2003**, *36*, 1923.
[11] K. X. Jin, S. G. Zhao, C. L. Chen, J. Y. Wang, *Materials Letters* **2008**, *62*, 1061.
[12] K. Vijayanandhini, T. R. N. Kutty, *J. Phys. D: Appl. Phys.* **2006**, *39*, 2902.
[13] B. S. Kang, H. Wang, J. L. MacManus-Driscoll, Y. Li, Q. X. Jia, *Appl. Phys. Lett.* **2006**, *88*, 192514.
[14] J. Li, Q. Huang, Z. W. Li, L. P. You, S. Y. Xu, C. K. Ong, *J. Appl. Phys.* **2001**, *89*, 7428.
[15] A. Hammouche, E. Siebert, A. Hammou, *Materials Research Bulletin* **1989**, *24*, 367.
[16] H. L. Ju, J. Gopalakrishnan, J. L. Peng, Oi Li, G. C. Xiong, T. Venkatesan, R. L. Greene, *Phys. Rev. B* **1995**, *51*, 6143.
[17] M. H. Kane, K. Shalini, C. J. Summers, R. Varatharajan, J. Nause, C. R. Vestal, Z. J. Zhang, I. T. Ferguson, *J. Appl. Phys.* **2005**, *97*, 023906.
[18] K. Vijayanandhini, T. R. N. Kutty, *Solid State Communications* **2007**, *141*, 252.
[19] X. Liu, Z. Jiao, K. Nakamura, T. Hatano, Y. Zeng, *J. Appl. Phys.* **2000**, *87*, 2431.
[20] J.-H. Park, E. Vescovo, H.-J. Kim, C. Kwon, R. Ramesh, T. Venkatesan, *Phys. Rev. Lett.* **1998**, *81*, 1953.

[21] T.-Y. Cai, S. Ju, Z.-Y. Li, *Phys. Rev. B* **2005**, *71*, 224417.
[22] L. Ranno, A. Llobet, R. Tiron, E. Favre-Nicolin, Applied *Surface Science* **2002**, *188*, 170.
[23] M. Rajeswari, R. Shreekala, A. Goyal, S. E. Lofland, S. M. Bhagat, K. Ghosh, R. P. Sharma, R. L. Greene, R. Ramesh, T. Venkatesan, T. Boettcher, *Appl. Phys. Lett.* **1998**, *73*, 2672.
[24] A. Gupta, G. Q. Gong, G. Xiao, P. R. Duncombe, P. Lecoeur, P. Trouilloud, Y. Y. Wang, V. P. Dravid, J. Z. Sun, *Phys. Rev. B* **1996**, *54*, R15629.
[25] D. Das, C. M. Srivastava, D. Bahadur, A. K. Nigam, S. K. Malik, *J. Phys.: Condens Matter.* **2004**, *16*, 4089.
[26] Ll. Balcells, J. Fontcuberta, B. Martínez, X. Obradors, *Phys. Rev. B* **1998**, *58*, R14697.
[27] T. Y. Koo, S. H. Park, K.-B. Lee, Y. H. Jeong, *Appl. Phys. Lett.* **1997**, *71*, 977.
[28] Q. Huang, J. Li, X. J. Huang, C. K. Ong, X. S. Gao, *J. Appl. Phys.* **2001**, *90*, 2924.
[29] X. W. Li, A. Gupta, G. Xiao, G. Q. Gong, *Appl. Phys. Lett.* **1997**, *71*, 1124.
[30] K.-K. Choi, T. Taniyama, Y. Yamazaki, *J. Appl. Phys.* **2001**, *90*, 6145.
[31] S. Valencia, O. Castanõ, J. Fontcuberta, B. Martínez, Ll. Balcells, *J. Appl. Phys.* **2003**, *94*, 2524.
[32] K. Dörr, T. Walter, M. Sahana, K.-H. Müller, K. Nenkov, K. Brand, L. Schultz, *J. Appl. Phys.* **2001**, *89*, 6973.
[33] H. Gao, W. Cai, P. Shimpi, H.-J. Lin, P.-X. Gao, *J. Phys. D: Appl. Phys.* **2010**, *43*, 272002.